ELSEVIER

Journal of Chromatography A, 779 (1997) 91–112

JOURNAL OF CHROMATOGRAPHY A

Characterization of liquid chromatographic stationary phases by Raman spectroscopy Effect of ligand type

Charles A. Doyle[a], Thomas J. Vickers[b], Charles K. Mann[b], John G. Dorsey[b,*]

[a]*Department of Chemistry, University of Cincinnati, Cincinnati, OH 45221-0172, USA*

[b]*Department of Chemistry, Florida State University, Tallahassee, FL 32306-4390, USA*

Received 9 December 1996; received in revised form 1 April 1997; accepted 7 April 1997

Abstract

This study represents the first Raman spectroscopic characterization of conventional chemically-bonded liquid chromatographic (LC) stationary phases under typical flow-rate and pressure conditions. Raman spectra were obtained for amino propyl (NH_2), cyano propyl (CN), phenyl (Ph), octadecyl (C_{18}), octyl (C_8), and methyl (C_1) chemically-bonded silica-based stationary phases in 100% aqueous mobile phases. The present experimental set-up has allowed Raman spectra of various stationary phase ligands, present in sub-monolayer coverages on the siliceous supports, to be obtained. This study: (1) demonstrates that conventional Raman spectroscopic techniques can be used to study LC stationary phases; (2) presents the experimental set-up, conditions, and approaches utilized to obtain Raman spectra of conventional stationary phases; (3) examines the spectroscopic differences observed for a variety of different types of bonded ligands that are typically used in reversed-phase (RPLC) and normal-phase (NPLC) liquid chromatographic separations; and (4) considers other future studies that are possible with this experimental approach, including mobile phase composition and temperature studies. © 1997 Elsevier Science B.V.

Keywords: Stationary phases, LC; Raman spectroscopy; Ligand orientation

1. Introduction

In this study Raman spectroscopy is used to examine bonded stationary phase ligands present in sub-monolayer coverages on siliceous supports. This is unique in that it represents the first time that Raman spectroscopy has been used to characterize conventional chemically-bonded LC stationary phases under typical flow-rate and pressure conditions. In addition, these direct, on-column, noninvasive measurements represent the first spectroscopic study to examine chemically-bonded LC stationary phases wetted by 100% water at conventional LC flow-rates and back pressures.

A variety of spectroscopic techniques have been used to examine the surface species present on both bare and bonded silica-based chromatographic supports and related substrates. These techniques include, among others, ultraviolet–visible absorbance (UV–Vis), fluorescence, electron spin resonance (ESR), nuclear magnetic resonance (NMR), infrared (IR), and to a much lesser extent, Raman spec-

*Corresponding author.

0021-9673/97/$17.00
PII S0021-9673(97)00404-4

troscopies. UV–Vis and fluorescence [1], and NMR and ESR [2,3] spectroscopic investigations of chromatographic stationary phases have recently been thoroughly reviewed. In addition, a summary of vibrational studies which have examined chromatographic stationary phases and related substrates is presented below. These techniques have provided supporting and complementary qualitative and, in some cases, quantitative information about the types, relative quantities, distributions, conformations, dynamics, and reactivities of surface species on chromatographic supports. The combination of information obtained from spectroscopic and chromatographic studies has provided insights into stationary phase synthesis and stability, as well as into the interactions involved in solute retention. Although much information has been obtained about stationary phases and the overall retention process, a detailed understanding of the mechanisms of solute retention is still elusive [4,5].

1.1. Characterization of surface silanols and other silica features

An area of interest that a major portion of previous infrared studies has examined is the types of silanol groups present on different types of siliceous surfaces and their reactivities toward various adsorbates and organosilane molecules. The surface of the hydrophilic silica particles consists of siloxanes (≡Si-O-Si≡), several different types of silanol groups, and depending on conditions, various quantities of surface-adsorbed water. The different types of silanols include free, isolated, single, or lone silanols (≡SiOH); internally hydrogen-bonded, bridged, vicinal, or associated silanols (=Si(OH)-O-(HO)Si=); and silanediols or geminal silanols ($=Si(OH)_2$) [6–10]. Hydrogen bonding, or bridging, of adjacent silanols is assumed to occur for those silanols that are in close proximity to one another (2.4 to 3.1 Å apart), whereas silanols that are farther apart than 3.1 Å from their nearest neighboring silanols are referred to as isolated, or free, silanols [11,12]. The terminology used to identify different types of silanols often depends upon a particular author's preference, and probably results from the inability of any one experimental technique to unambiguously differentiate among the various types. The variable terminology can sometimes present confusion when comparing results from different research groups. For example, Köhler et al. [13] use the term 'isolated' to include both single and geminal silanols, whereas Sagliano, et al. [14] use 'isolated' to denote lone, or 'one', silanols. Hair and Hertl [15] use 'free' to designate either single or geminal silanols. Miller et al. [16] use the term 'single' to denote both vicinal and lone silanols because each type has only one hydroxyl group per silicon atom.

Infrared spectra in the fundamental region, 4000 to about 700 cm^{-1}, generally contain a sharp absorption band at about 3750 cm^{-1} attributed to single silanols and, for fully hydrated silica, a broad set of features covering the region below 3750 cm^{-1} down to as low as 2800 cm^{-1} which results from the overlap of several broad bands due to various forms of hydrogen-bonded silanols and adsorbed water. The broadness of these features is attributed in part to hydrogen-bonding, which is a general phenomenon that tends to cause band-broadening for other functional groups as well as hydroxyls, and the fact that there is probably a distribution of vicinal silanols [11,15] with proximities (or bond distances) varying between 2.4 and 3.1 Å. The absorption of infrared radiation at the lower frequencies is attributed to those silanols that are closer to one another and thus under the influence of stronger hydrogen-bonding interactions.

Band assignments for the various features observed in the OH stretching region below about 3750 cm^{-1} are summarized below. An absorption band at about 3720 cm^{-1} has been assigned to 'terminal' silanols [17–22], in which the silanol oxygen is hydrogen-bonded to the hydrogen of another silanol, but the 'terminal' hydrogen of this silanol is free from hydrogen bonding. A broad band with an absorption maximum near 3660 cm^{-1} has been assigned to weakly hydrogen-bonded vicinals [11,14,18,23–26] or to inaccessible, or buried, silanols referred to as 'internal' silanols [22,27–29]. A broad band with a maximum at about 3550 to 3500 cm^{-1} has been assigned to strongly hydrogen-bonded vicinal groups [17,21–23,27,28,30–32], water hydrogen-bonded to surface hydroxyls [14,26], or to both of these groups [23,25]. A broad OH stretching band due to physisorbed water absorbs in

the region 3500 to 3400 cm^{-1} and is also associated with a water deformation at about 1640 to 1630 cm^{-1} [6,7,17,24,25,33–35].

The assignment of infrared bands to geminal silanols has been more difficult. Generally, geminal silanols are assumed to absorb infrared radiation at wavenumber values closer to those of single silanols than vicinal silanols [13,18,19,21,26], but absorption at 3500 cm^{-1} has also been attributed to geminal silanols [34,36]. Hair and Hertl [26] resolved three bands at 3751, 3747, and 3743 cm^{-1} which were assigned to single (3747 cm^{-1}) and geminal (3751 and 3743 cm^{-1}) silanols. Spectroscopic evidence for the existence of geminal silanols is more clearly provided by ^{29}Si cross-polarization magic-angle-spinning nuclear magnetic resonance spectroscopy (^{29}Si CP–MAS NMR) studies [13,37], which differentiates between silicon atoms with one hydroxyl group attached (single silanols) and silicon atoms with two hydroxyl groups present (geminal silanols), but does not provide any indication of the extent of hydrogen-bonding among various surface hydroxyl groups.

The adsorptive and reactive behavior of the various types of silanol groups has been investigated by infrared spectroscopy under a variety of conditions. Infrared spectroscopy has been used to monitor the effects of exposure of silica to various molecular species. These species have included: water [12,15,17,19,21,23,32,36,38–40]; ethers [15,20,23]; alcohols [15,23,41]; ammonia [15,17,25]; aniline, acetone, benzene, and triethylamine [15]; pyridine [15,42]; hydrogen chloride, chlorine, carbon tetrachloride and silicon tetrachloride [25]; boron trichloride [22,28,29]; and titanium tetrachloride, dimethyl zinc, and trimethyl aluminum [22]. Exposure to isotopic species have included molecular deuterium [25]; deuterium oxide [18,20,22,23,25, 27,28,30,32,33,38]; deuterated ammonia [17,22]; deuterated alcohols [22]; and $H_2{}^{18}O$ [17]. The reactivity of the various silanols to different organosilanes [11–14,18,22,26,30,31,35,39,40,43–45] is especially relevant to the synthesis and applications of reversed-phase stationary phases. Hertl and Hair [46] examined the effect of the adsorption of twenty-three different compounds on the frequency shift of the 3750 cm^{-1} surface silanol group band position.

Marshall et al. [43] synthesized octadecyl (C_{18}) stationary phases with improved chromatographic efficiencies by 'precapping' a small population, about 5%, of highly reactive silanols. Diffuse-reflectance infrared Fourier-transform spectroscopy (DRIFTS) studies suggested that the precapping occurred with a chemically distinct subset population of associated silanols. Through DRIFTS and other measurements, Sagliano et al. [14] found that the hydrolytic stability of monomeric C_4 stationary phases depended on the starting silica. DRIFTS measurements revealed that isolated (and/or geminal) silanols were not only among the first to react during silanization, but in the case of one of the starting silicas which had been exposed to sodium sulfate during manufacture, these same silanol sites, in the form of bonded siloxane species, were also more reactive toward hydrolysis and thus reappeared upon removal of bonded-alkyl ligands. Using multiple spectroscopic techniques, including DRIFTS, along with chromatographic, thermogravimetric (TGA), and other analytical methods of analysis, Köhler et al. [13] characterized the hydrolytic stabilities of different C_1 stationary phases, and their reactivities towards basic organic compounds. Their results indicated that isolated, non-hydrogen-bridged, highly acidic silanol groups were responsible for the adsorption of basic compounds and for the low hydrolytic stability of alkyl bonded-phase ligands.

Besides O-H stretching in the fundamental region, the near infrared (NIR) region from 8000 to 4000 cm^{-1} has also been examined with regards to silica and bonded-phase characterization [32,47–52]. This spectral region offers the advantage that combination (stretching and bending modes) absorption bands for silanols and physically adsorbed water are resolved in this region. Only a few infrared studies have examined the low wavenumber region in any detail because silica and other oxides are opaque to infrared radiation below about 1350 cm^{-1} [21,35,53–55], particularly for transmission studies involving relatively thick silica samples such as self-supporting pressed disks and pellets (typically 5 to 40 mg/cm^2) [35,54,55]. This spectral region contains information about the skeletal vibrations of the SiO_2 bulk material, surface siloxane groups, Si-O stretching of surface hydroxyl groups, and Si-C and Si-Cl stretching bands of modified silicas. Transmission thin film

techniques (approximately 0.2 mg/cm^2) [35] and DRIFTS [56] were used to examine this spectral region. Another drawback of using pressed pellets is that the number of internal silanols and the amount of interparticle hydrogen bonding increases with increases in the pressure used to form the pellets [11,21–23,28,38].

Oxide materials, however, are relatively poor Raman scatterers [54,55] and therefore the spectral region below about 1350 cm^{-1} is more accessible for siliceous samples using Raman spectroscopy. A number of Raman studies have examined this low wavenumber spectral region for siliceous materials [53,57–62]. Fewer Raman studies have examined the O–H stretching region for surface silanol characterization [58–60,62]. Koenig et al. [53] correlated vibrations in the O–H stretching region obtained by infrared spectroscopy with vibrations in the Si–O stretching region obtained from Raman studies. Additional Raman investigations have examined the adsorptive and reactive behavior of different siliceous materials upon exposure to molecular hydrogen and deuterium [59]; benzene [63,64]; pyridine [63,65–67]; water [62]; ammonia, trimethylchlorosilane, and vinyltriethoxysilane [53]; acetone, aniline, benzylamine, chlorobenzene, dioxane, furan, and methyl iodide [63]; hexamethyldisilazane, titanium tetrachloride, trimethyl aluminum, silicon tetrachloride, germanium tetrachloride, chloromethylsilanes, and chloromethyl–germanium compounds [55].

1.2. Verification of surface derivatization

Vibrational spectroscopic techniques have also been used as a diagnostic tool to verify that chemical derivatization of the substrate surface has been achieved following synthesis. IR has been used to identify characteristic bands due to different functional groups of various organosilane ligands bonded to chromatographic surfaces including alkyl [68–71], allyl [69], aminoalkyl [68,72], cyanoalkyl [68], methacryloxyalkyl [72], phenyl phases [68,69,73,74], and mixed-bonded phases containing both alkyl and cyanoalkyl ligands [75]. IR has also been used to verify the conversion of aminoalkyl-bonded ligands to various bonded zwitterionic-exchangers [76,77], amino acid-bonded phases [78,79], immobilized artificial membrane-bonded phases [80–82] and other functional groups [83] by the formation of amide linkages.

Pesek and coworkers have utilized DRIFTS to characterize modified substrate surfaces and various bonded phases prepared by unique synthetic procedures which are not typically used for the syntheses of liquid chromatographic stationary phases. They examined the preparation and stability of silica hydride-modified intermediate substrates [84], as well as the reaction of these substrates with terminal olefins to produce alkyl- [85] and diol-bonded [86] phases. Similar alkyl-bonded phases produced by olefin hydrosilation of silicon hydride-modified alumina [87,88], zirconia, thoria, and titania [88] substrates were also characterized by DRIFTS. In addition, allyl-bonded silica-based stationary phases [89,90] produced by surface chlorination of the substrate followed by a Grignard reaction, and the subsequent conversion of the allyl-bonded phase to a cation-exchange material [90] were examined by DRIFTS. They also characterized various chemically-bonded liquid crystal materials by infrared spectroscopic techniques [91–93].

1.3. Investigations of alkyl chain conformations

The vast majority of the above vibrational studies have examined dry powdered samples or dry samples compressed into either pellets or thin films. Vapor phase dosing of these samples with molecules of interest was the primary means by which the adsorptive/reactive behavior of these samples was investigated. Only a limited number of vibrational studies have examined the conformational behavior of the stationary phase ligands [94–99]. Several of these vibrational investigations have varied the solvent composition [94–96,99] or temperature [94] to examine the conformation of the bonded ligands under various conditions simulating chromatographic environments. These studies have also included the comparison of spectral features due to the bonded ligands with those of neat alkanes [94,98] and silanes [97,99] to decipher the orientations of the ligands, the effects of various solvents, and the influence of temperature on the conformations.

Sander et al. [94] used transmission Fourier-transform infrared spectroscopy (FTIR) to examine alkyl

chain conformations of monomeric bonded ligands with chain lengths from C_1 to C_{22} as a function of temperature and solvent composition. The dry-bonded phases were compared to the free silanes of corresponding chain length at ambient temperature, and as a function of temperature for the C_{18} and C_{22} stationary phases. They used the normal coordinate calculations of Snyder [100] for *n*-alkanes based on the rotational isomeric state model [101,102], to assign spectral features, and to obtain semiquantitative estimates of the degree of chain dissorder, or the number and types of gauche defects, for the various matrices. They found that the bonded-alkyl chains exhibited conformational disorders (gauche defects or bending of chains) comparable to the corresponding liquid *n*-alkanes. The bonded-alkyl chains exhibited increased chain ordering in the presence of different solvent mixtures and also with decreasing temperature for the dry-bonded phases, but were not observed to undergo 'phase transitions' comparable to that observed for free alkanes and silanes.

Thompson and Pemberton [99] demonstrated the feasibility of examining alkylsilane layers covalently bound to silica surfaces using Raman spectroscopy. Due to the fact that Raman scattering is an inherently weak phenomenon, they utilized a surface enhanced Raman spectroscopic (SERS) approach by using an elaborately prepared layered 'sandwich' structure. This sandwich structure consisted of a smooth silver surface, which provided the SERS signal enhancement, to which a self-assembled layer of (3-mercaptopropyl)trimethoxysilane (3MPT) was attached; followed by spin coating a sol–gel solution onto the 3MPT-modified silver surface to produce a thin silica layer; and subsequent reaction of this silica layer with octadecyltrichlorosilane.

They observed that, although the presence of minimal gauche defect structure was evident, the dry surface bound alkyl chains of the sandwich film appeared to adopt a predominantly ordered configuration similar to that of solid octadecyltrichlorosilane, as opposed to disordered liquid silane [99]. The presence of the various solvents including acetonitrile, deuterated methanol, and water, induced only subtle conformational changes of the bonded-alkyl chains. Acetonitrile was found to provide greater mobility of the alkyl chains than deuterated methanol, and the organic solvents appeared to disrupt the alkyl chains more significantly than water.

The above mentioned vibrational conformation studies have provided useful insights into the orientations of bonded ligands under various conditions, and have been a motivating factor in the present research. These previous conformation studies either examined dry stationary phases [94,96–99] or stationary phases solvated under static flow conditions at atmospheric pressure [94–96,99] to simulate liquid chromatographic environments. In addition, several of the subtrates were flat surfaces [96,97,99] rather than chromatographic particles. The present study, and future studies employing this new on-column technique, offer the advantage that conventional chromatographic stationary phases are being examined under conditions where the stationary phase ligands are solvated using typical mobile phase flow-rates and column back pressures. Stationary phase ligand solvation under pressurized conditions is particularly important when examining the effects of high aqueous content mobile phases, because the hydrophobic bonded ligands are not easily wetted.

The present studies represent the first time that Raman spectroscopy has been used to characterize conventional chemically-bonded liquid chromatographic stationary phases under typical flow-rate and pressure conditions. Presumably, similar Raman studies have not been reported prior to this because strong overlapping fluorescence signals from the siliceous support typically interfere with the weaker Raman signals of the bonded ligands. Raman scattering is an inherently weak phenomenon and it has been estimated that only about 10^{-8} of the incident photons undergo Raman scattering [103]. Raman spectroscopic investigations of silicas are generally plagued by fluorescence interferences [54,55,61–64,99], although silica (SiO_2) itself is not inherently fluorescent. The fluorescence is usually attributed to the presence of aromatic impurities either adsorbed to, or associated with, trace metal impurities in the silica. The different quantities, typically about 0.1–0.3% for chromatographic grade silica [8,9,13,104–109], and types of metal impurities usually result from differences in the silica manufacturing methods employed. Various approaches to reducing fluorescence interferences in Raman spectroscopic studies

have included pre-irradiating, or laser-bleaching, the sample to burn off fluorescence [61,62], and silica thermal pretreatments *in vacuo* to 350°C [62], in oxygen to 500°C [63,64,66], and in air to 600°C [54] and 700°C [55]. In the present study, the standard practice of equilibrating the stationary phase with an organic solvent, such as methanol or acetonitrile, following column packing simultaneously rinses away organic impurities that cause fluorescence interferences, enabling the weak Raman spectral features due to the bonded ligands to be obtained.

2. Experimental

2.1. Instrumentation

The Raman–liquid chromatography experimental setup is depicted in Fig. 1a, and consists of the combination of conventional HPLC equipment and a dispersive Raman spectrometer equipped with a fiber optic probe. The liquid chromatograph in Fig. 1a illustrates the setup in what would be its most complicated form, in that, for example, an injector and detector are only needed when solute interactions are to be considered, and a thermostatted precolumn is only needed for mobile phase temperature equilibration. The present study examines stationary phase–mobile phase interactions under ambient temperature conditions, and the precolumn, injector, and UV–Vis absorbance detector were not used. A Spectra-Physics SP8800 ternary HPLC pump (ThermoSeparations, San Jose, CA, USA) was used to pump the desired mobile phase through a custom-built Raman–LC column packed with the appropriate stationary phase. An additional Raman cell (not shown in Fig. 1) was also used for static liquid and solid measurements (Raman liquid–solid cell) and was constructed in a similar fashion to the Raman–LC column (detailed description to follow).

An expanded view of a Raman–LC column used in these studies is shown in Fig. 1b. These columns were built 'in house' and are constructed from polished and acid-washed stainless steel chromatographic tubing (1/4 in. O.D. and 4.6 mm I.D.; 1 in. = 2.54 cm) (Alltech Associates, Deerfield, IL, USA) and standard 1/4 in. LC column endfittings (Upchurch Scientific, Oak Harbor, WA, USA). The

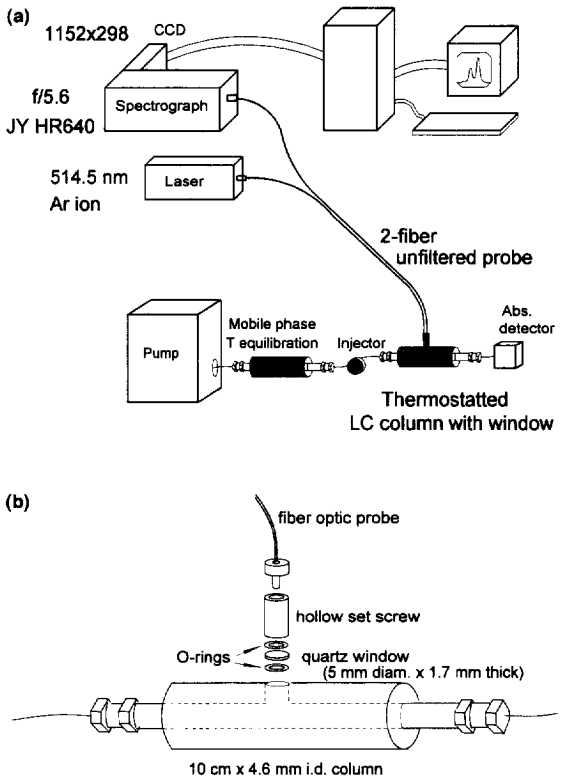

Fig. 1. (a) The liquid chromatography–Raman spectroscopy experimental system. This configuration allows direct, non-invasive, spectroscopic observation of conventional LC stationary phases under conditions typically employed in liquid chromatographic experiments. (See Section 2.1 for a detailed description of the experimental setup). (b) An expanded view of a 'custom-built' Raman–LC column used to directly examine different chemically-bonded liquid chromatographic stationary phases under typical, packed-bed, LC conditions. (See Section 2.1 for a detailed description).

on-column spectroscopic viewing area was constructed from a solid block of stainless steel and is similar to a hollow 'T'-type fitting to which two pieces of the aforementioned stainless steel tubing were welded in series, to either end of this 'T' fitting, being careful to minimize the introduction of possible dead volume sources. The total column length can be made to nearly any size desired, but the overall column length used in these studies was 10 cm.

The third opening of this 'T' fitting, normal to the direction of mobile phase flow, was machined so as to provide a metal ridge near the junction of the 'T'

opening to retain an optical viewing window and O-rings. Lead O-rings (3.0 mm I.D.×5.3 mm O.D.× 0.92 mm thick) sandwich either face of a quartz disk (5.0 mm diameter×1.7 mm thick) viewing window. The upper portion of this opening of the 'T' fitting is threaded to accept a hollow set screw which holds the lead O-rings and quartz window in place, producing a seal that is able to withstand conventional LC 'back' pressures. Teflon O-rings have also been tested. The teflon O-rings were easier to use in the assembly and disassembly of the columns and cells and provided better seals than the lead O-rings, but also contributed spectral interferences, and were therefore not used in the present study.

The Raman liquid–solid cell used for static measurements utilizes a similar design to hold an identical quartz window in place at the bottom of a well (5/8 in. I.D.×2.5 in. high) constructed from stainless steel that allows coolant to be circulated between the inner and outer walls of the container. This cell is equipped with a removable lid that remains in place during temperature equilibration, but is removed during spectroscopic measurements so that the lid does not scatter incident radiation.

The Raman spectroscopic portion of this experimental set-up has been previously described in detail [110,111]. Briefly, the radiation (514.5 nm) used to excite the mobile phase–stationary phase sample matrix is produced by an Argon ion laser (Stabilite 2017 with a 2550 Controller; Spectra-Physics, Mountain View, CA, USA) operating at a power of 150 mW at the fiber tip, and is directed into the sample mixture by a 400-μm diameter core all-silica optical fiber. The second fiber of the bifurcated fiber-optic probe collects the scattered radiation and directs it to the entrance optics of a Jobin Yvon HR640 spectrograph (Instruments SA, Edison, NJ, USA). The entrance slit width of the spectrograph is 200 μm for the C–H stretching spectral region and 300 μm for the C–C stretching and C–H bending region. Each leg of the probe is about one meter in length. The end of the fiber–optic probe is equipped with a standard SMA fitting which allows the probe to be attached to the hollow set screw of a particular cell and fixes the position of the probe tip to be flush with, and only slightly offset from, the surface of the quartz window. There is no filtering in the probe to reject the Raman signal produced by the siliceous optical fibers. The scattered radiation is dispersed by a grating onto an 1152×298 pixel liquid nitrogen-cooled charge coupled device (CCD) detector (Princeton Instruments, Trenton, NJ, USA). A 600 grooves per mm grating is used for the C–H stretching spectral region and a 1200 grooves per mm grating is used for the C–C stretching and C–H bending region. All 298 pixels of the CCD are binned in the direction parallel to slit height. The collected signals are digitized and transferred to an IBM compatible personal computer, which also controls data collection for data treatment, using software developed 'in-house'.

2.2. Stationary phases and reagents

Conventional, silica-based, chemically-bonded liquid chromatographic stationary phases used in these studies include: octadecyl (C_{18}), octyl (C_8), methyl (C_1), cyano propyl (CN), amino propyl (NH_2), and phenyl (Ph) ligands. All phases used were synthesized from monofunctional silanes except for the phenyl phase, which was synthesized from the difunctional reactant 2-phenylpropyldichlorosilane.

The stationary phases investigated are listed in Table 1, and are either commercially available, Symmetry and μBondapak phases (Waters Corporation, Milford, MA, USA), or were synthesized 'in house' from commercially available starting silica, Davisil (Davison Chemical, Baltimore, MD, USA) and Microporasil (Waters Corporation) using established synthetic procedures [112,113]. Table 1 also lists physical properties, provided by the manufacturers, of the different starting silicas and stationary phases. Bonding densities reported in Table 1 pertain to the primary ligands of interest only (listed in the first column of the Table 1), and do not include the bonding densities of the endcapping ligands.

The bonding density, or chain density, is a measure of the number of silane ligand molecules attached directly to a given area of the support surface, and strictly speaking is only valid for monofunctional ligands, which are only able to react with hydroxyl sites (silanols) on the surface of the siliceous support. The bonding density reported for the difunctional phenyl phase (Table 1) is probably not a completely accurate descriptor of the surface-bonded chain density in this case. For ease of

Table 1
Chromatographic stationary phases investigated

Phase[a]	Bonding density (μmol m^{-2})	End-capped	Particle shape/size	Pore size (Å)	Surface area (m^2 g^{-1})
Symmetry C_{18}	~3.2	yes	Spherical/5 μm	90	340
Symmetry C_8	~3.4	yes			
μBondapak C_{18}	~1.5	yes	Irregular/10 μm	125	300
μBondapak NH_2	[c]	no			
μBondapak CN	[c]	yes			
μBondapak phenyl[b]	~3	yes			
Microporasil C_{18}	3.52	no	Irregular/6–10 μm	125	311
Microporasil C_{18}	2.34	no			
Microporasil C_{18}	1.68	no			
Davisil C_1	3.77	yes	Irregular/20–30 μm	147	300
Bare Spherisorb	(n.a.)	no	Spherical/10 μm	300	150

[a] Phases are mono-functional unless noted otherwise[b].
[b] Difunctional phase.
[c] Proprietary information, not provided by manufacturer.
n.a. = Not applicable.

comparison only, the 'bonding density' of this polymeric stationary phase is reported to allow a convenient means of comparing monomeric and polymeric stationary phases.

Both reflux and ultrasound synthetic methods [112] were used to prepare the various Microporasil and Davisil stationary phases. The ultrasound method, in conjunction with 4-dimethylaminopyridine (4-DMAP) as an acid acceptor and catalyst, produces stationary phases with consistently higher ligand-bonding densities than typically achieved using conventional reflux procedures. Whereas bonding densities of commercially available monomeric C_{18} stationary phases are typically between 2.5 and 3.2 μmol m^{-2} [69,112,114,115], the highest bonding densities for monomeric C_{18} stationary phases achieved to date, as high as 4.4 μmol m^{-2}, resulted from the ultrasound procedure [112,116].

The different stationary phase materials were packed into individual Raman–LC columns by slurry packing techniques using an air-driven pump (Alltech Associates). Following column packing, the stationary phases were equilibrated by passing at least 500 ml of 100% acetonitrile through each column, then gradually changing the mobile phase composition from 100% acetonitrile to 100% water over about a 6-h time period (at a flow-rate of 1 ml min^{-1}), and finally equilibrating the stationary phases with at least 1 l of water at a flow-rate of 1 ml min^{-1} before the spectroscopic investigations. HPLC grade acetonitrile (Fisher Scientific, Atlanta, GA, USA) and distilled water which had been further purified by passage through a Barnstead Nanopure II water purification system (Barnstead Company, Newton, MA, USA) equipped with a 0.45-μm filter, were used as equilibrating and mobile phase solvents. In addition, HPLC grade toluene (Fisher Scientific) was used to evaluate the spectral features of the phenyl stationary phase.

3. Results and discussion

3.1. Demonstration of spectral subtractions

Raman spectra of several different sample matrices are presented in Fig. 2A and Fig. 3A for the C–C stretching and C–H bending region (low wavenumber region) and the C–H stretching region (high wavenumber region), respectively. Unsub-

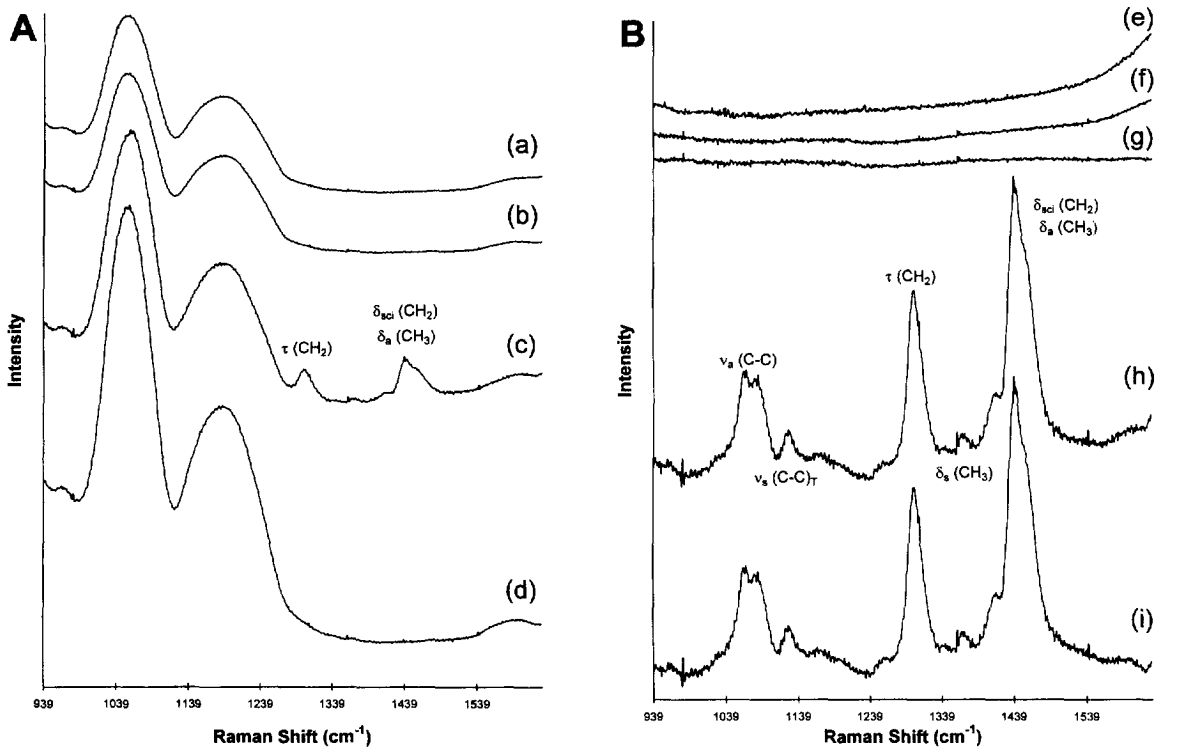

Fig. 2. (A) Raw, unsubtracted, Raman vibrational spectral features in the C–C stretching and C–H bending region due to various sample matrices and the fiber-optic probe. (a) Features due to water and the fiber-optic probe. (b) Features due to bare Spherisorb silica, water, and the fiber-optic probe. (c) Features due to the 3.52 μmol m^{-2} Microporasil C_{18} stationary phase, water, and the fiber-optic probe. (d) Features due only to the fiber-optic probe. (B) Raman spectral features in the C–C stretching and C–H bending region following subtraction of spectral features due to individual components in the sample matrices. (e) Features due only to water, after subtraction of the fiber-optic probe spectral features in d (e = a − d). (f) Features due to bare Spherisorb silica and water, after subtraction of the fiber-optic probe spectral features in d (f = b − d). (g) Features due only to bare Spherisorb silica, after subtraction of features due to the fiber-optic probe (spectrum d) and to water (spectrum e) (g = b − d − e). (h) Features due to the 3.52 μmol m^{-2} Microporasil C_{18} stationary phase and water, after subtraction of the fiber-optic probe spectral features in d (h = c − d). (i) Features due only to the 3.52 μmol m^{-2} Microporasil C_{18} stationary phase, after subtraction of features due to the fiber-optic probe (spectrum d) and to water (spectrum e) (i = c − d − e).

tracted spectra for (a) water, (b) bare Spherisorb silica in water, (c) the 3.52 μmol m^{-2} Microporasil C_{18} stationary phase in water, and (d) the siliceous fiber-optic probe are presented for both spectral regions (Fig. 2A, Fig. 3A). The probe consists of two siliceous optical fibers and has its own characteristic Raman-scattering spectral features (spectrum d of Fig. 2A, Fig. 3A). The fiber-optic probe spectra were obtained by scattering the incident radiation off solid potassium chloride, which is a good scattering medium and yet contributes no Raman spectral features of its own in the spectral regions of interest. Identical spectral features would also be obtained by scattering the incident radiation off of a metal surface, which also would not contribute to the spectral features observed in these regions. The spectra in (a) and (d) of Fig. 2A and Fig. 3A were obtained using the Raman liquid–solid cell and no solvent flow. The spectra of the stationary phases (spectra b and c) were obtained using Raman–LC columns (as illustrated in Fig. 1) packed with the appropriate stationary phases and under dynamic flow conditions of 1.0 ml min^{-1} of the 100% aqueous mobile phase. A total data acquisition time of 10 min was used for all stationary phases packed in the Raman–LC columns, whereas 5 min was used for

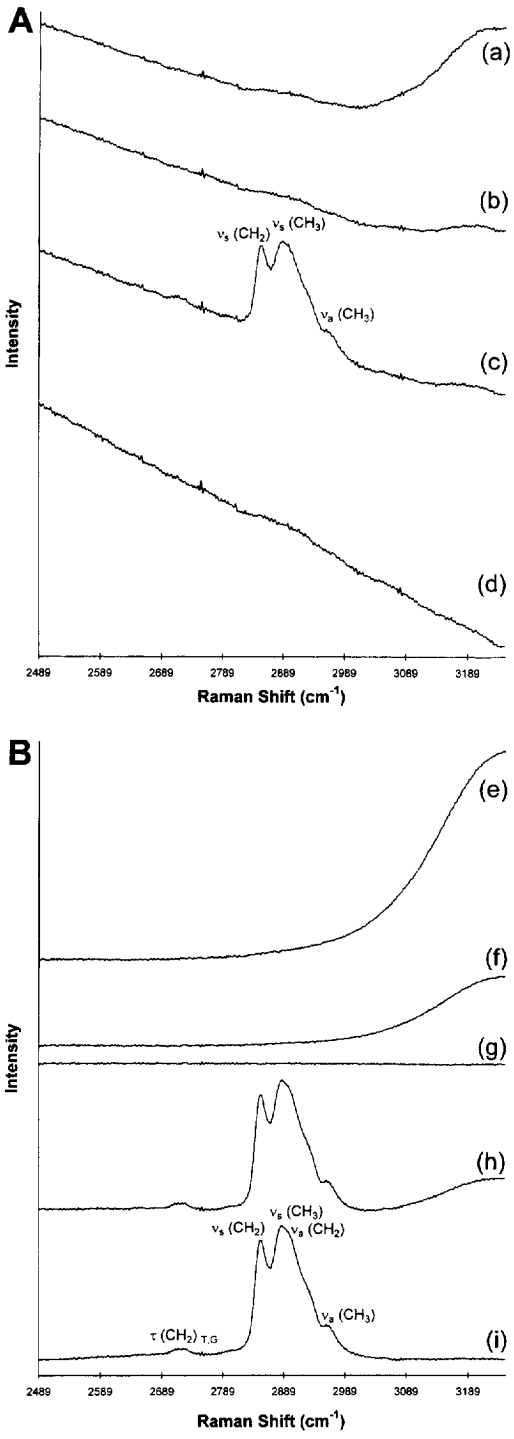

Fig. 3. (A) Same as Fig. 2A, except that the spectral region is the C–H stretching region. (B) Same as Fig. 2B, except that the spectral region is the C–H stretching region.

the probe spectra obtained using solid potassium chloride, and 3 min was used for all static liquid measurements.

In the low wavenumber region (Fig. 2A) the major spectral features present at 1057 and 1184 cm^{-1} in each spectrum (a–d) are silica features (Si–O stretching) due primarily to the fiber-optic probe (spectrum d), and/or the chromatographic silica substrates for spectra b and c. The relative shapes of these two major spectral features are the same in each of the spectra (a–d) of Fig. 2A. The only other immediately discernible features in Fig. 2A are the hydrocarbon features present in the spectrum of the bonded stationary phase (spectrum c) at 1300 and 1440 cm^{-1}. These hydrocarbon features are due to methylene twisting and to a combination of methyl asymmetric bending and methylene scissoring, respectively. The hydrocarbon features for this particular stationary phase (a high bonding density phase) were among the most prominent bonded phase spectral features observed, and for many stationary phases, the hydrocarbon features were not evident until after spectral subtraction (as illustrated in Fig. 2B). The relative intensity differences (shown to scale) observed in each of the spectra of Fig. 2A are due to the different scattering cross sections of the liquid (a), the 'wetted' stationary phases (b and c), and the dry solid (d).

Unlike in the C–C stretching and C–H bending region, the spectrum due to the fiber-optic probe lacks any significant spectral features in the C–H stretching region (spectrum d of Fig. 3A). The major spectral features observed in the C–H stretching region (Fig. 3A) are the sigmoidal feature in the range 2990 to 3250 cm^{-1} of spectrum (a) due to water, and the hydrocarbon features in the range 2830 to 2990 cm^{-1} of spectrum (c) due to the 3.52 $\mu mol\ m^{-2}$ Microporasil C_{18} stationary phase ligands. Bands characteristic of CH_2 symmetric stretching (2852 cm^{-1}) and CH_3 asymmetric stretching (2961 cm^{-1}) are present, as well as a broad band at 2889 cm^{-1} which probably results from overlapping features due to CH_3 symmetric stretching (typically at 2872 cm^{-1} for free alkanes) and CH_2 asymmetric stretching (typically at 2926 cm^{-1} for free alkanes) [117,118]. Typical band assignments for nitrile-substituted hydrocarbons, saturated hydrocarbons and monosubstituted aromatic hydrocarbons are summa-

rized for the low and high wavenumber spectral regions in Table 2 Table 3, respectively.

Subtraction of the spectral features due to the fiber-optic probe allow spectral features of the chromatographic sample matrices to be more readily observed (Fig. 2B, Fig. 3B). In the low wavenumber region (Fig. 2B), the water spectrum (e), obtained by subtracting spectrum (d) from spectrum (a) (i.e., e = a − d), has no significant spectral features, except for the gradually increasing intensity observed in the range 1420 to 1629 cm^{-1}. A similar, but more gradual increase in intensity is observed for the spectrum of the bare Spherisorb silica in the presence of the water mobile phase (spectrum f). Subtraction of the water features (spectrum e) from this bare Spherisorb silica/water spectrum (f) gives the resulting spectrum due only to the bare Spherisorb silica (spectrum g). Due to the lack of characteristic spectral features in spectrum g, it is evident that the chromatographic silica gel matrix contributes no additional features to the spectra observed, once the spectra have been corrected for the siliceous fiber-optic probe (spectrum d). A similar result is obtained in the C–H stretching region (spectrum g of Fig. 3B), and indicates that the use of the present fiber-optic probe experimental setup to directly examine surface silanol features due to the siliceous chromatographic support material would probably not be feasible.

Spectral differences would be expected in comparing fused-silica fibers to amorphous chromatographic silica particles. One possible reason for the lack of differences between the spectral features observed for the silica fibers and the chromatographic silica, as indicated by the lack of spectral features in spectrum g of Fig. 2B and Fig. 3B, may have to do with the quantities of material being examined. Silica is a relatively weak scatterer, but in the case of the fiber spectrum (particularly in the low wavenumber region (spectrum d of Fig. 2A)), the prominence of the silica features results from sampling the entire 2 m of both the excitation and collection fibers. On the other

Table 2
Typical band assignments in the C–C stretching and C–H bending region for nitrile-substituted hydrocarbons, saturated hydrocarbons, and mono-substituted aromatic hydrocarbons

Raman shift (cm^{-1})	Notation	Description	Reference
Nitrile compounds			
1405–1435	δ (R-CH_2-CN)	methylene deformation in R-CH_2-CN	[117]
Saturated hydrocarbons			
1040–1100	ν_a (C–C)	carbon–carbon asymmetric stretching	[117]
1065	ν_a $(C–C)_T$	C-C asymmetric stretching ('trans' conformations)	[99]
1080	ν $(C–C)_G$	C–C stretching ('gauche' conformations)	[99]
1120–1180	ν_s (C–C)	carbon–carbon symmetric stretching	[117]
1124	ν_s $(C–C)_T$	C–C symmetric stretching ('trans' conformations)	[99]
1295–1305	τ (CH_2)	methylene -$(CH_2)_n$- in-phase twisting	[117]
1370–1380	δ_s (CH_3)	methyl symmetric bending	[117,118]
1440–1470	δ_a (CH_3)	methyl asymmetric bending	[117,118]
1445–1475	δ_{sci} (CH_2)	methylene scissoring	[117,118]
Mono-substituted aromatic hydrocarbons			
990–1010	ν $(C–C)_{breath}$	mixing of in-phase ring stretching (or 'breathing') and in-plane ring bending	[117]
1027	ν $(C–C)_{circ}$	mixing of 'semi-circle' stretching and in-plane CH bending	[117]
1146–1166	δ_a $(C–C)_{ip}$	asymmetric CH in-plane bending	[117]
1170–1180	δ_s $(C–C)_{ip}$	symmetric CH in-plane bending	[117]
1208	ν (C_{aryl}–CH_3)	methyl–phenyl stretch (substituent sensitive)	[117]
1565–1590	ν_a $(C–C)_{quad}$	carbon–carbon asymmetric 'quadrant' ring stretching	[117]
1585–1620	ν_s $(C–C)_{quad}$	carbon–carbon symmetric 'quadrant' ring stretching	[117]

Table 3
Typical band assignments in the C–H stretching region for nitrile-substituted hydrocarbons, saturated hydrocarbons, and mono-substituted aromatic hydrocarbons

Raman shift (cm^{-1})	Notation	Description	Reference
Nitrile compounds			
2230–2260	ν (CN)	C≡N (or C–CN) stretching	[117,118]
Saturated hydrocarbons			
2724	$\tau\ (CH_2)_{T,G}$	methylene twisting	[99]
2843–2863	$\nu_s\ (CH_2)$	methylene symmetric stretching	[99,117,118]
2862–2882	$\nu_s\ (CH_3)$	methyl symmetric stretching	[117,118]
2890	$\nu_a\ (CH_2)$	methylene asymmetric stretching	[99]
2916–2936	$\nu_a\ (CH_2)$	methylene asymmetric stretching	[117,118]
2927	$\nu_s\ (CH_2)_{FR}$	methylene free rotation	[99]
2952–2972	$\nu_a\ (CH_3)$	methyl asymmetric stretching	[117,118]
2957	$\nu_s\ (CH_3)$	methyl symmetric stretching	[99]
Mono-substituted aromatic hydrocarbons			
3030–3070	$\nu_{aryl}\ (CH)$	aromatic (or aryl) C–H stretching	[117,118]

hand, since the diameter of the Raman–LC column is only 4.6 mm, only a small volume of chromatographic silica is being sampled. Thus, although spectral differences may exist between these two different types of silica, the differences are not observed because of the relatively small quantity of chromatographic silica being sampled in comparison to the 2 meters of silica fiber being sampled in the case of the fiber optic probe.

Spectra h and i of Fig. 2B are for the 3.52 $\mu mol\ m^{-2}$ Microporasil C_{18} stationary phase in the presence of the water mobile phase (spectrum h) and for the bonded phase after subtraction of water spectral features (spectrum i). Since the chromatographic silica is not contributing any new characteristic spectral features (spectrum g), the features present in spectrum i are due only to the bonded-octadecylsilyl ligands, and not to the siliceous support matrix. Bands characteristic of carbon–carbon asymmetric (1072 cm^{-1}) and symmetric (1123 cm^{-1}) stretching, $-(CH_2)_n-$ in-phase twisting (1300 cm^{-1}), and CH_3 symmetric bending (1368 cm^{-1}) and the combination of CH_2 scissoring and CH_3 asymmetric bending (1440 cm^{-1}) are present. The band due to carbon–carbon symmetric stretching is extremely sensitive to the physical state of free alkanes and alkyl silanes, and has been attributed to result from the alignment of the chain carbons in a linear, or '*trans*', configuration [99].

Probe-subtracted spectra of the C–H stretching region are presented in Fig. 3B. Spectral features due to water (spectrum e) are significantly more intense in the C–H stretching region (Fig. 3B), relative to the hydrocarbon features (spectra h and i), than in the C–C stretching and C–H bending region (Fig. 2B). Nonetheless, the sigmoidal water feature (OH stretching region) is easily removed from the bonded-hydrocarbon features in the high wavenumber region. Spectrum g of Fig. 3B, again demonstrates that characteristic spectral features due to the bare chromatographic stationary phase do not significantly differ from those features obtained for the siliceous fiber-optic probe, and thus a flat baseline is obtained for the spectral features of the bare chromatographic silica (spectrum g) once the probe (spectrum d) and water (spectrum e) features have been removed.

As noted for Fig. 3A, characteristic hydrocarbon features are again observed in the high wavenumber region (Fig. 3B) for the octadecylsilyl ligands of the 3.52 $\mu mol/m^2$ Microporasil C_{18} stationary phase (spectra h and i). After subtraction of the fiber-optic probe features, the weak band characteristic of methylene twisting (2720 cm^{-1}) becomes evident, in addition to the features already noted earlier. There are slight discrepancies in the band assignments published for this region. Thompson and Pemberton [99] assign features at 2890 cm^{-1} and 2927 cm^{-1} to methylene asymmetric stretching and methylene free

rotations, respectively. In the present study, the broad band at about 2890 cm^{-1} is attributed to both methylene asymmetric stretching, as well as to the symmetric stretching of methyl groups. Methylene asymmetric stretching is more typically assigned to spectral features in the region 2916 to 2936 cm^{-1} and methyl group symmetric stretching is typically observed in the region 2862 to 2882 cm^{-1} [117,118] for hydrocarbons. The assignment of the band intensity at approximately 2890 cm^{-1} will be discussed in more detail with regards to Fig. 9. In addition, Thompson and Pemberton assign the band at 2957 cm^{-1} to the symmetric stretching of the methyl groups for their octadecylsilyl-bonded sandwich films [99]. However, this band at about 2957 cm^{-1} is more typically assigned to the asymmetric stretching of methyl groups [117,118].

As can be seen from the comparison of spectral features due to water (spectra e of Fig. 2B and Fig. 3B) and to the bonded-octadecylsilyl ligands (spectra i of Fig. 2B and Fig. 3B), water is a convenient mobile phase from a spectroscopic standpoint because the mobile phase spectral features do not significantly overlap the features due to the bonded ligands. More importantly, water was selected as the mobile phase in this initial study to demonstrate the utility of the current experimental arrangement for expanding upon the solvent-dependent transmission FTIR studies of Sander et al. [94]. They used deuterium oxide–deuterated methanol solutions, from 0 to 30% deuterium oxide (D_2O), to examine the effect of solvent mixtures on C_{18} bonded-phase ligand conformations. Because chemically-bonded stationary phases are very hydrophobic, especially alkyl phases, 'wetting' of the stationary phase ligands with water is extremely difficult and typically must be done under the high pressures obtainable using LC pumps and columns, but even then only after an extended period of equilibration. Presumably, Sander et al. [94] were unable to wet the stationary phase ligands with solvent mixtures of higher aqueous content because their phases were wetted by capillary action at atmospheric pressure. The present on-column study is in fact the first time that bonded chromatographic stationary phases wetted by 100% water have been examined by any spectroscopic technique at conventional LC flow-rates and back pressures. Bliesner and Sentell [119] were the first to wet the stationary phase ligands with 100% water (D_2O) under pressurized conditions prior to spectroscopic analysis. They wetted the stationary phase ligands using a packed LC column, but then unpacked the stationary phase from the column in order to perform NMR analyses.

In the present study the term 'wetting' should be taken to mean that the stationary phase has been fully equilibrated with the 100% aqueous mobile phase, with at least 1 l of water at a flow-rate of 1 ml min^{-1}. The conformation of stationary phase ligands, in particular alkyl-bonded ligands, is presumed to vary with the percentage organic content of the mobile phase. In high organic content mobile phases, the bonded ligands are wetted by organic molecules and thus extend away from the support surface. In high aqueous content mobile phases, anywhere from about 45–100% water for C_{18} ligands in water–methanol mobile phases depending on the equilibration history [120], the alkyl ligands collapse on the silica surface. This conformational change is currently under investigation using the on-column Raman spectroscopy set-up presented herein.

3.2. Raman spectral features due to NH_2-, CN-, and Ph-bonded ligands

Figs. 4 and 5 compare the spectral features due only to the ligands of (a) the 2.34 μmol m^{-2} Microporasil C_{18} stationary phase, (b) the μBondapak NH_2 stationary phase, (c) the μBondapak CN stationary phase, (d) the μBondapak Phenyl stationary phase, and to (e) neat liquid toluene in the low and high wavenumber regions, respectively. Spectral features due to the fiber-optic probe, and the aqueous mobile phase for spectra a–d, have already been removed. First, comparison of the octadecylsilyl spectral features due to the 2.34 μmol m^{-2} Microporasil C_{18} stationary phase (spectrum a of Fig. 4 and Fig. 5) to the features due to the 3.52 μmol m^{-2} Microporasil C_{18} stationary phase (spectrum i of Fig. 2B and Fig. 3B) demonstrates that the octadecylsilyl-bonded ligand features are reproducible for different bonding density stationary phases. This point will be further demonstrated in Figs. 6 and 7.

Comparison of the octadecylsilyl features to those

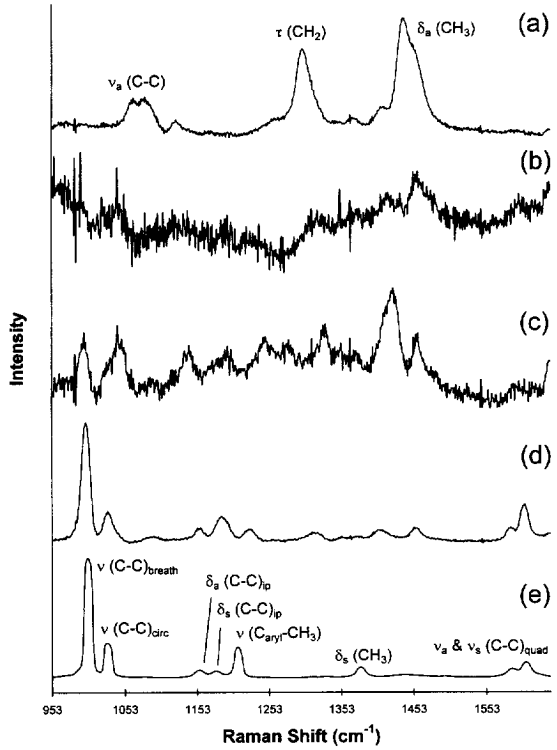

Fig. 4. Raman spectral features in the C–C stretching and C–H bending region due to the bonded ligands of (a) the 2.34 μmol m^{-2} Microporasil C_{18} stationary phase, (b) the μBondapak NH_2 stationary phase, (c) the μBondapak CN stationary phase, (d) the μBondapak Phenyl stationary phase, and (e) neat liquid toluene. Features due to the water mobile phase (1.0 ml min^{-1} flow-rate) (spectra a–d) and the siliceous fiber-optic probe (see Fig. 2) have been subtracted to obtain features due only to the stationary phase ligands (spectra a–d) and neat liquid toluene (spectrum e).

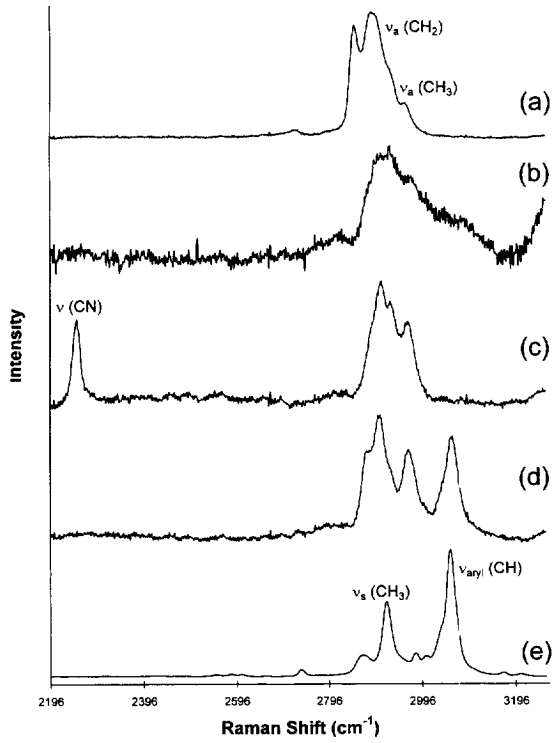

Fig. 5. Same as Fig. 4, except that the spectral region is the C–H stretching region.

of the amino, cyano and phenyl phases (Figs. 4 and 5) demonstrates, not too surprisingly, that different spectral features are observed for the different types of bonded ligands. In both Figs. 4 and 5, the spectra have been scaled to the same size as the most prominent spectrum (spectrum e) to more clearly illustrate the differences in the spectral features due to the different ligands. A comparison of the signal-to-noise ratio in the different spectra provides some visualization of the relative intensities of the different spectral features. In the low wavenumber region (Fig. 4), the different spectra have been multiplied by the following scaling factors: (a)×108.7, (b)×1497, (c)×452.1, (d)×78.44, and (e)×1. In the high wavenumber region (Fig. 5), the different spectra have been multiplied by the following scaling factors: (a)×10.64, (b)×418.6, (c)×42.80, (d)×41.54, and (e)×1.

Features due to the NH_2 stationary phase (spectrum b of Figs. 4 and 5) are very weak, especially in the low wavenumber region, and originate from the $-CH_2-$ groups of the propyl spacer in the spectral regions examined. Features due to the CN stationary phase (spectrum c of Figs. 4 and 5) are slightly more prominent than the features observed for the amino propyl ligands. In the low wavenumber region (Fig. 4), both the NH_2 and CN phases exhibit bands at 1457 cm^{-1} consistent with methylene scissoring vibrations, and the CN phase has an additional more prominent feature at 1425 cm^{-1} due to R-CH_2-CN methylene deformations [117]. The CN phase has several additional spectral features in the low wavenumber region that are presumably due to various other carbon, methylene, and nitrile interactions, including bands at 995 and 1044 cm^{-1} that are

possibly due to carbon–carbon stretching modes that have shifted in the presence of the nitrile group. In the high wavenumber region (Fig. 5), again the NH_2 phase spectral features are very weak. The CN phase exhibits a band at 2252 cm^{-1} characteristic of the C–N stretching of nitrile compounds. In the C–H stretching region, the features due to the cyano phase are sharper than those due to the amino phase, but both spectra suggest that in addition to methylene stretching vibrations (at 2908 and 2928 cm^{-1} for the cyano phase), the spectra also indicate the presence of methyl asymmetric stretching features (at 2965 cm^{-1} for the cyano phase). This indicates that the bands in this region are due not only to the methylene groups in the propyl spacer chains of both phases, but also to the methyl groups attached to the silicon atoms that anchor the ligands to the chromatographic silica surface. This result would also indicate that the low wavenumber region spectra (Fig. 4) of these phases may also have some features due to these silicon attached methyl groups.

The phenyl stationary phase produced spectral features (spectrum d of Figs. 4 and 5) with band positions resembling those typically observed for monosubstituted aromatic species, for example neat toluene (spectrum e of Figs. 4 and 5). In the low wavenumber region, both spectra exhibit bands at about 1000, 1028, 1587, and 1605 cm^{-1} due to in-phase ring stretching (breathing), 'semi-circle' stretching, and asymmetric and symmetric 'quadrant' ring stretching of the mono-substituted phenyl rings, respectively [117]. The band at 1209 cm^{-1} in the toluene spectrum is indicative of an aryl–methyl stretch. For toluene, this band is the third, and most prominent band, of a series of three bands in the spectral region between 1125 to 1250 cm^{-1}. The position of this band is very substituent sensitive [117]. Therefore, it is not too surprising to observe that, for the phenyl phase it is the middle band at about 1187 cm^{-1} which is the most prominent band of this three band series. This band is probably due to the aryl–methine stretching occurring in the phenyl phase. Additionally, the phenyl phase exhibits more prominent saturated hydrocarbon features than toluene (on a relative basis) at 1317, 1405 and 1456 cm^{-1} as a result of the propyl spacer substituted at the second position by the phenyl group in the case of the bonded phase.

In the high wavenumber region (Fig. 5), both the phenyl phase (spectrum d) and toluene (spectrum e) exhibit aryl ring C–H stretching features at about 3058 cm^{-1}, but the features in the saturated hydrocarbon region (below 3000 cm^{-1}) are considerably different for the two phases. Toluene exhibits essentially only one other strong band at about 2919 cm^{-1}, due to the symmetric stretching of the methyl group. The phenyl phase, however, exhibits a prominent band at about 2905 cm^{-1} due to the C–H stretching of the methine group directly attached to the phenyl ring. Also evident in the saturated hydrocarbon stretching region for the phenyl phase is a prominent shoulder at 2881 cm^{-1} due to methylene stretching, and a band at 2967 cm^{-1} probably due to a combination of asymmetric methyl stretching resulting from the terminal methyl groups of the phenyl spacers and the methyl groups attached to the silicon atoms that anchor the ligands to the chromatographic silica surface.

3.3. Raman spectral features due to various alkyl-bonded ligands

Figs. 6 and 7 compare the spectral features observed in the low and high wavenumber regions, respectively, for the various octadecyl and octyl stationary phases investigated. Raman spectral features due only to bonded ligands of (a) the 1.68, 2.34, and 3.52 $\mu mol\ m^{-2}$ Microporasil C_{18} stationary phases; (b) the Symmetry C_{18} stationary phase; (c) the Symmetry C_8 stationary phase; and (d) the μBondapak C_{18} stationary phase are presented in Figs. 6 and 7. The spectra presented in Fig. 6a and Fig. 7a are unscaled (×1) to demonstrate the effect of ligand-bonding density on the relative intensities and overall shapes of the observed spectral features. The other spectra (spectra b–d) have been scaled to the same size as the spectral features observed for the 3.52 $\mu mol\ m^{-2}$ Microporasil C_{18} stationary phase, which are the most prominent features in the spectra of Fig. 6a and Fig. 7a. In the low wavenumber region (Fig. 6), the different spectra have been multiplied by the following scaling factors: (a)×1, (b)×1.038, (c)×3.793, and (d)×3.490. In the high wavenumber region (Fig. 7), the different spectra have been multiplied by the following scaling

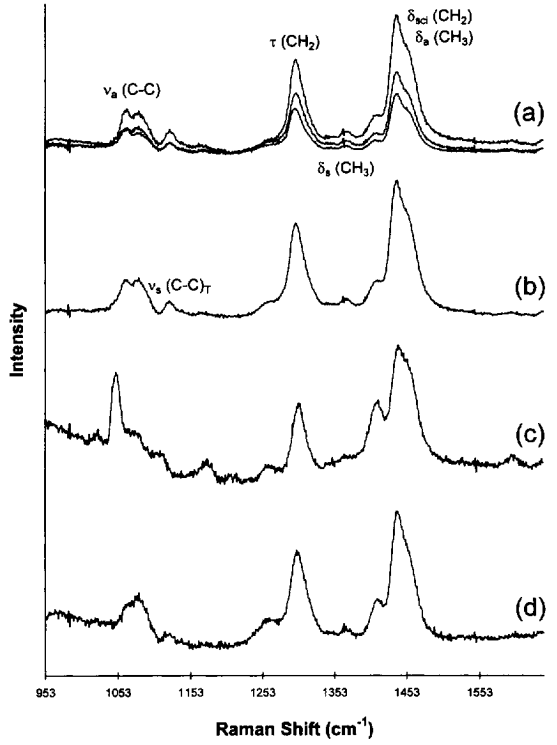

Fig. 6. Raman spectral features due to alkyl-bonded LC stationary phase ligands in the C–C stretching and C–H bending region. Raman spectral features due to (a) the 1.68, 2.34, and 3.52 μmol m^{-2} Microporasil C_{18} stationary phases; (b) the Symmetry C_{18} stationary phase; (c) the Symmetry C_8 stationary phase; and (d) the μBondapak C_{18} stationary phase. Features due to the water mobile phase (1.0 ml min flow-rate) and the siliceous fiber-optic probe (see Fig. 2) have been subtracted to obtain features due only to the stationary phase ligands.

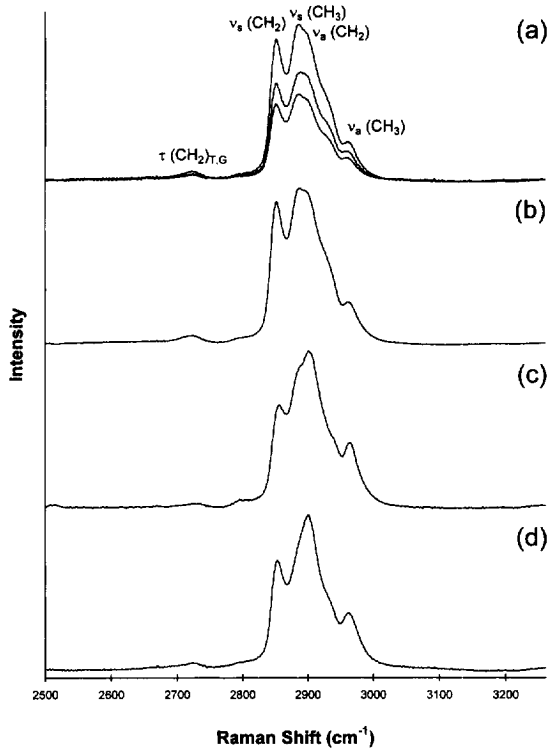

Fig. 7. Same as Fig. 6, except that the spectral region is the C–H stretching region.

factors: (a)×1, (b)×0.8299, (c)×2.198, and (d)×2.281.

The effect of C_{18} ligand-bonding density on the relative intensities and overall peak shapes of the spectral features can readily been seen in the spectra of Fig. 6a and Fig. 7a. The Microporasil stationary phases were synthesized from the same lot of starting silica, to aid in the comparison of the spectral features. In both the C–C stretching and C–H bending region and the C–H stretching region, the same overall spectral features are present for each stationary phase, but their relative intensities decrease with decreasing ligand-bonding density. Peak intensities are linearly related to octadecyl bonding density for the Microporasil C_{18} phases, with linear correlation coefficients ranging from 0.967 to 1.000 for the peaks in the C–H bending and C–H stretching regions. The lower correlation coefficients were obtained in the C–H bending region due to the higher noise levels in this region. Comparison of the spectral features and relative band intensities of the Symmetry C_{18} stationary phase (spectrum b) to those of the various Microporasil C_{18} stationary phases (spectra a) shows that comparable spectra were obtained for these different phases.

Not too surprisingly, the spectral features due to the octylsilyl ligands (spectrum c of Figs. 6 and 7) are different from those observed for the octadecylsilyl ligands presented in spectra a and b. For example, in the low wavenumber region (Fig. 6), the octyl phase (spectrum c) exhibits a sharp band at about 1049 cm^{-1} due to carbon–carbon stretching, whereas the octadecyl phases (spectra a and b) exhibit broader and relatively less intense overlapping bands at about 1063 and 1078 cm^{-1}. The

differences in relative band intensities and band positions of other spectral features are more readily compared by reporting the ratio of intensities (I) of the two bands of interest at their respective wavenumber values (in cm^{-1}) of maximum intensity (I_{max1}/I_{max2}). For instance, the methylene twisting band at about 1300 cm^{-1} is a relatively weaker feature, compared to the band at about 1440 cm^{-1} due to the combination of methyl asymmetric bending and methylene scissoring, and its maximum is shifted to higher energy by about 5 cm^{-1} for the Symmetry C_8 phase compared to the Symmetry C_{18} phase. The relative intensity of these two bands is $I_{1440}/I_{1299}=1.53$ and $I_{1441}/I_{1304}=1.75$ for the Symmetry C_{18} and C_8 phases, respectively. The as yet unassigned band at 1411 cm^{-1} for the octyl phase is significantly more prominent than the corresponding feature appearing in the Symmetry C_{18} spectrum as a weak shoulder at about 1413 cm^{-1}. The relative intensity of this band to that of the band at about 1440 cm^{-1} is $I_{1440}/I_{1413}=4.97$ and $I_{1441}/I_{1411}=2.07$ for the Symmetry C_{18} and C_8 phases, respectively.

In the high wavenumber region (Fig. 7), the methylene symmetric stretching band at about 2855 cm^{-1} is weaker, and the methyl asymmetric stretching band at about 2962 cm^{-1} is stronger for the octyl phase (spectrum c) than that observed for the octadecyl phases (spectra a and b) relative to the band intensity due to the combination of methyl symmetric stretching and methylene asymmetric stretching at roughly 2894 cm^{-1}. In addition, the maxima of the spectral features due to methylene symmetric stretching, to the combination of methyl symmetric stretching and methylene asymmetric stretching, and to methyl asymmetric stretching for the octyl phase are shifted to higher energies by 5, 14, and 3 cm^{-1}, respectively, in comparison to those observed for the Symmetry C_{18} stationary phase. The intensities of the symmetric methylene stretching and methyl asymmetric stretching bands relative to the band due to the combination of methyl symmetric stretching and methylene asymmetric stretching are $I_{2887}/I_{2852}=1.10$ and $I_{2887}/I_{2962}=3.82$ for the Symmetry C_{18} phase and $I_{2901}/I_{2857}=1.54$ and $I_{2901}/I_{2965}=2.42$ for the Symmetry C_8 phase, respectively.

However, the spectral features due to the μBondapak C_{18} stationary phase (spectrum d of Figs. 6 and 7) differ significantly, especially in the C–H stretching region, compared to the features obtained for the other octadecyl stationary phases (spectra a and b of Figs. 6 and 7). In fact, the spectral features due to the μBondapak C_{18} phase appear to more closely resemble those of the octyl phase than the other octadecyl phases, particularly in the high wavenumber region. In the low wavenumber region (Fig. 6), the methylene twisting band is more prominent, relative to the band resulting from methyl asymmetric bending and methylene scissoring, for the μBondapak C_{18} phase ($I_{1440}/I_{1301}=1.44$) than for either the Symmetry C_8 or the C_{18} stationary phases, whereas the as yet unidentified band at 1413 cm^{-1} is relatively more prominent for the μBondapak C_{18} stationary phase ($I_{1440}/I_{1413}=3.56$) than for the Symmetry C_{18} stationary phase, but less prominent on a relative basis than that of the Symmetry C_8 stationary phase. In the high wavenumber region (Fig. 7), the μBondapak C_{18} stationary phase peak intensity maxima positions for methylene symmetric and methyl asymmetric stretching were at the same locations as those observed for the Symmetry C_{18} stationary phase, but the maximum of the band resulting from the combination of methyl symmetric and methylene asymmetric stretching was at the same location observed for the Symmetry C_8 stationary phase. The relative band intensities of the μBondapak C_{18} stationary phase ($I_{2901}/I_{2852}=1.43$ and $I_{2901}/I_{2962}=2.79$) more closely resemble those observed for the Symmetry C_8 stationary phase than those for the Symmetry C_{18} stationary phase.

A possible explanation for the spectral differences observed for the different octadecyl stationary phases is that, in some cases, spectral features due to endcapping ligands might be more prominent, and thus the spectral features observed could be the result of overlapping features from both the octadecyldimethylsilyl ligands and the trimethylsilyl ligands. Due to steric hindrance, only about 25 to 50% of the silanol groups present on the silica surface (approximately 8 ± 1 μmol m^{-2} on chromatographic-grade silica [7,121,122]) react with organosilanes. Typical bonding densities achieved in monomeric syntheses of C_{18} materials are between 2.5 and 3.2 μmol m^{-2}, and are somewhat higher for shorter alkyl chains. Due to steric effects, the maximum coverage obtainable using an octa-

decyldimethylsilane, for example, is considered to be approximately 4.0–4.7 μmol m^{-2}. Sentell and Henderson [116] recently obtained one of the highest bonding densities reported for a monomeric C_{18} stationary phase (4.4 μmol m^{-2}).

The Microporasil C_{18} stationary phases are all non-endcapped stationary phases of varying octadecyldimethylsilyl ligand density. The octadecyldimethylsilyl ligand density of 3.52 μmol m^{-2} is considered to be a 'high' bonding density monofunctional, or monomeric, stationary phase. Bonding densities of 2.34 μmol m^{-2} and 1.68 μmol m^{-2} C_{18} are considered to be medium/low and low bonding densities, respectively. In the case of the endcapped Symmetry C_{18} stationary phase, the C_{18} bonding density of ~3.2 μmol m^{-2} is considered to be a medium–high bonding density, whereas for the endcapped μBondapak C_{18} stationary phase the C_{18} bonding density of ~1.5 μmol m^{-2} is extremely low. A further explanation as to why the spectral features for the endcapped Symmetry C_{18} stationary phase do not appear to differ from the features obtained for the non-endcapped Microporasil C_{18} stationary phases, whereas those of the endcapped μBondapak C_{18} stationary phase vary significantly compared to the other octadecyl phases, might have to do with the relative quantity of endcapping ligands present on each stationary phase.

3.4. Raman spectral features due to trimethylsilyl endcapping ligands

To investigate the above hypothesis about the spectral differences observed for the different octadecyl stationary phases, a trimethylchlorosilyl (C_1) stationary phase was synthesized and Raman spectra obtained for this stationary phase as well. In Figs. 8 and 9, the spectral features due to (a) the ~1.5 μmol m^{-2} Bondapak C_{18} endcapped stationary phase and (b) the 2.34 μmol m^{-2} Microporasil C_{18} non-endcapped stationary phase are again presented for both the low and high wavenumber regions. Spectrum c shows the spectral features remaining after subtracting the octadecyl spectral features due to the nonendcapped C_{18} stationary phase (spectrum b) from those of the endcapped C_{18} stationary phase (spectrum a). Assuming that this hypothesis about the endcapping ligands is correct, these resulting spectral

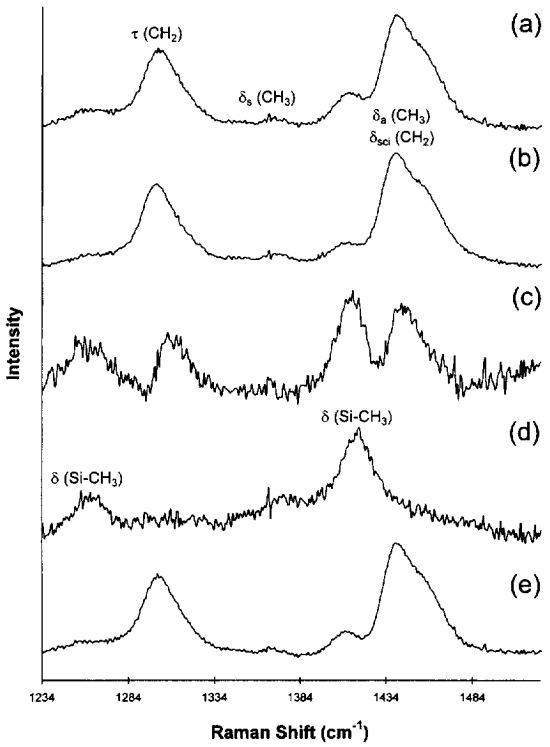

Fig. 8. Examination of Raman spectral features due to the endcapping ligands of selected alkyl-bonded LC stationary phases. Features due to the water mobile phase (1.0 ml min^{-1} flow-rate) and the siliceous fiber-optic probe (see Fig. 2) have been subtracted to obtain features due only to the stationary phase ligands. Raman spectral features due to (a) the ~1.5 μmol m^{-2} Bondapak C_{18} endcapped stationary phase; and (b) the 2.34 μmol m^{-2} Microporasil C_{18} non-endcapped stationary phase. (c) Remaining spectral features after subtracting octadecyl spectral features due to the non-endcapped C_{18} stationary phase (spectrum b) from those of the endcapped C_{18} stationary phase (spectrum a) (c = a − b). (d) Raman spectral features due to the 3.77 μmol m^{-2} Spherisorb C_1 stationary phase. (e) Remaining spectral features after subtracting trimethylsilyl spectral features due to the C_1 stationary phase (spectrum d) from those of the endcapped C_{18} stationary phase (spectrum a) (e = a − d).

features (spectrum c) should be due only to the endcapping ligands of the ~1.5 μmol m^{-2} Bondapak C_{18} stationary phase. For comparison, the spectral features due to the 3.77 μmol m^{-2} Davisil C_1 stationary phase are presented in spectrum d. In both spectral regions, the 'endcapped-nonendcapped' spectrum (spectrum c) and C_1 bonded phase spectrum (spectrum d) contain similar features, and the differences between spectra c and d appear to be

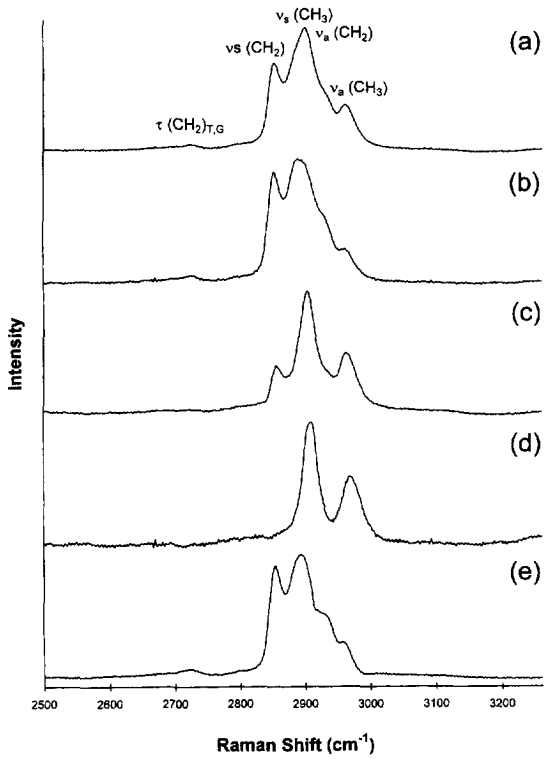

Fig. 9. Same as Fig. 8, except that the spectral region is the C–H stretching region.

attributable to residual methylene features present in the 'endcapped–nonendcapped' spectrum that are not present in the C_1 bonded phase spectrum.

In the low wavenumber region (Fig. 9) spectrum d contains two features at 1261 and 1418 cm^{-1} due to methyl–silicon deformations. Spectrum c contains similar features at 1260 and 1414 cm^{-1}, with additional features at 1308 and 1443 cm^{-1}. Therefore the band observed at about 1413 cm^{-1} for both endcapped and nonendcapped octadecyldimethylsilyl-bonded phases, and even the octyl-bonded phase, results in part from the methyl–silicon deformations of the octadecyl- and octyldimethylsilyl ligands and any trimethylsilyl endcapping ligands present. The residual bands at 1308 and 1443 cm^{-1} of spectrum c are consistent with methylene twisting and methylene scissoring features that have been shifted by a few wavenumbers from values typically observed for saturated hydrocarbons. In the high wavenumber region (Fig. 9), the spectrum due to the C_1 bonded phase (spectrum d) contains two bands at 2908 and 2968 cm^{-1} due to methyl symmetric and asymmetric stretching, respectively. The methyl symmetric stretching band is significantly displaced from that observed for saturated hydrocarbons (2862–2882 cm^{-1}) because of its direct attachment to a silicon atom. The methyl asymmetric stretching band position is more consistent with that observed for saturated hydrocarbons (2952–2972 cm^{-1}). Spectrum c contains similar features at 2902 and 2962 cm^{-1}, as well as a band at 2855 cm^{-1} consistent with methylene symmetric stretching and evidence for residual methylene asymmetric stretching as well. The valley between the two peaks observed for the C_1 stationary phase (spectrum d) more nearly approaches baseline resolution than the same region for spectrum c, indicating the presence of residual methylene asymmetric stretching features in this region after subtraction of nonendcapped C_{18} spectral features from the endcapped C_{18} spectral features. These residual methylene features suggest that some of the methylene groups of the octadecyl chain are in a different environment, spectroscopically, than the bulk of the methylene groups in a given octadecylsilyl chain. The residual methylene features probably result from the methylene group directly attached to the surface bound silicon atom.

As a further comparison, the endcapping features from the C_1 stationary phase (spectrum d of Figs. 8 and 9) were also subtracted from the spectral features of the ~1.5 μmol m^{-2} μBondapak C_{18} endcapped stationary phase (spectrum a of Figs. 8 and 9), and the resulting spectral features, presumably due only to the octadecyl ligands of the μBondapak stationary phase, are presented in spectrum e. Comparison of these resulting spectral features (spectrum e), presumably due only to octadecylsilyl ligands, to the spectral features observed for a nonendcapped octadecylsilyl stationary phase (spectrum b) shows that overall, the features are again in pretty good agreement. Particularly in the high wavenumber region, the differences observed are again attributable to residual methylene groups, as indicated by the band shape differences in the asymmetric methylene stretching region. The spectra in Figs. 8 and 9 demonstrate that the spectral features observed for the ~1.5 μmol m^{-2} μBondapak C_{18} endcapped

stationary phase are the result of overlapping features from both the octadecyldimethylsilyl ligands and the trimethylsilyl endcapping ligands.

4. Summary and conclusions

The results presented here demonstrate that conventional Raman spectroscopic methods are feasible for direct examination of the bonded ligands on silica-based liquid chromatographic stationary phases, without the need for more elaborate systems, such as surface enhanced Raman spectroscopy (SERS). These initial studies demonstrate the capabilities of the present experimental setup for examining spectroscopic differences due to various chemically-bonded stationary phase ligands. Besides spectroscopically observable differences being detected for phases with different primary ligands, spectral subtraction verified that the spectral features observed for the ~1.5 μmol m^{-2} μBondapak C_{18} endcapped stationary phase were the result of overlapping features from the octadecyldimethylsilyl ligands and the trimethylsilyl ligands. In the case of the high-bonding density Symmetry C_8 endcapped stationary phase (spectrum c of Figs. 6 and 7), it is possible that some of the observed features are due to the endcapping ligands as well as the octyldimethylsilyl ligands. This would need to be investigated by comparing features from a nonendcapped C_8 stationary phase. At this point, we are assuming that the spectral features are due primarily to the octyldimethylsilyl ligands because features due to the endcapping ligands were not noticeable for the endcapped Symmetry C_{18} stationary phase with a primary ligand bonding density comparable to that of the Symmetry C_8 stationary phase.

The ability to obtain Raman spectral features of different ligands attached to chromatographic silica is significant considering that fluorescence interference is a major obstacle to such measurements. The present on-column experimental set-up provides a convenient means to obtain such spectral information. These on-column measurements offer the unique opportunity to obtain spectroscopic information about molecular-level changes occurring at the surface of chemically-bonded chromatographic stationary phases under typical conditions. The effects of mobile phase composition and thermal equilibration on the alkyl chain conformations of chemically-bonded liquid chromatographic stationary phases are currently under investigation.

Acknowledgments

The technical expertise of Mr. Keith Collins for assistance in the design and manufacture of the Raman–LC columns and the Raman liquid–solid cells employed in this study is gratefully acknowledged. The authors thank Dr. Raymond Crowley of Waters Corporation for providing the Symmetry and μBondapak stationary phases. The synthesis of the Microporasil C_{18} stationary phases by Ms. Jessica Wysocki is also gratefully acknowledged. The authors are grateful for support of this work by NIH GM-48561 and AFOSR, and J.G.D. is grateful to Merck Research Laboratories for continued support of our work.

References

[1] S.C. Rutan, J.M. Harris, J. Chromatogr. A 656 (1993) 197.
[2] K.B. Sentell, J. Chromatogr. A 656 (1993) 231.
[3] R.K. Gilpin, J. Chromatogr. A 656 (1993) 217.
[4] J.G. Dorsey, K.A. Dill, Chem. Rev. 89 (1989) 331.
[5] J.G. Dorsey, W.T. Cooper, Anal. Chem. 66 (1994) 857A.
[6] R.K. Iler, The Chemistry of Silica, John Wiley and Sons, New York, 1979.
[7] K.K. Unger, Porous Silica, Elsevier, Amsterdam, 1979.
[8] J. Nawrocki, Chromatographia 31 (1991) 177.
[9] J. Nawrocki, Chromatographia 31 (1991) 193.
[10] A. Berthod, J. Chromatogr. 549 (1991) 1.
[11] L.R. Snyder, J.W. Ward, J. Phys. Chem. 70 (1966) 3941.
[12] M. Mauss, H. Engelhardt, J. Chromatogr. 371 (1986) 235.
[13] J. Köhler, D.B. Chase, R.D. Farlee, A.J. Vega, J.J. Kirkland, J. Chromatogr. 352 (1986) 275.
[14] N. Sagliano Jr., R.A. Hartwick, R.E. Patterson, B.A. Woods, J.L. Bass, N.T. Miller, J. Chromatogr. 458 (1988) 225.
[15] M.L. Hair, W. Hertl, J. Phys. Chem. 73 (1969) 4269.
[16] M.L. Miller, R.W. Linton, G.E. Maciel, B.L. Hawkins, J. Chromatogr. 319 (1985) 9.
[17] B.A. Morrow, I.A. Cody, L.S.M. Lee, J. Phys. Chem. 80 (1976) 2761.
[18] A.J. van Roosmalen, J.C. Mol, J. Phys. Chem 82 (1978) 2748.
[19] A.J. van Roosmalen, J.C. Mol, J. Phys. Chem. 83 (1979) 2485.
[20] I. Tsuchlya, J. Phys. Chem. 86 (1982) 4107.

[21] P. Hoffman, E. Knözinger, Surf. Sci. 188 (1987) 181.
[22] B.A. Morrow, A.J. McFarlan, Langmuir 7 (1991) 1695.
[23] R.S. McDonald, J. Phys. Chem. 62 (1958) 1168.
[24] J.J. Fripiat, J. Uytterhoeven, J. Phys. Chem. 66 (1962) 800.
[25] J.B. Peri, J. Phys. Chem. 70 (1966) 2937.
[26] M.L. Hair, W. Hertl, J. Phys. Chem. 73 (1969) 2372.
[27] F.H. Hambleton, J.A. Hockey, J.A.G. Taylor, Trans. Faraday Soc. 62 (1966) 801.
[28] A.J. Tyler, F.H. Hambleton, J.A. Hockey, J. Catal. 13 (1969) 35.
[29] C.G. Armistead, A.J. Tyler, F.H. Hambleton, S.A. Mitchell, J.A. Hockey, J. Phys. Chem. 73 (1969) 3947.
[30] V.Y. Davydov, A.V. Kiselev, L.T. Zhuravlev, Trans. Faraday Soc. 60 (1964) 2254.
[31] S.P. Boudreau, W.T. Cooper, Anal. Chem. 61 (1989) 41.
[32] A. Burneau, O. Barrès, J.P. Gallas, J.C. Lavalley, Langmuir 6 (1990) 1364.
[33] J.J. Fripiat, M.C. Gastuche, R. Brichard, J. Phys. Chem. 66 (1962) 805.
[34] J.A. Hockey, Chem. Ind. (London) (1965) 57.
[35] C.P. Tripp, M.L. Hair, Langmuir 7 (1991) 923.
[36] J.A. Hockey, B.A. Pethica, Trans. Faraday Soc. 57 (1961) 2247.
[37] G.E. Maciel, D.W. Sindorf, J. Am. Chem. Soc. 102 (1980) 7606.
[38] F.H. Hambleton, J.A. Hockey, J.A.G. Taylor, Trans. Faraday Soc. 62 (1966) 795.
[39] J.P. Blitz, R.S.S. Murthy, D.E. Leyden, J. Colloid Interface Sci. 121 (1988) 63.
[40] C.P. Tripp, M.L. Hair, Langmuir 8 (1992) 1120.
[41] T.J. Horr, J. Ralston, R.S.C. Smart, Colloids Surf. 64 (1992) 67.
[42] D.E. Leyden, K.G. Proctor, in: H.E. Bergna (Ed.), The Colloid Chemistry of Silica, vol. 234, American Chemical Society, Washington D.C., 1994, pp. 257.
[43] D.B. Marshall, C.L. Cole, D.E. Connolly, J. Chromatogr. 361 (1986) 71.
[44] C.P. Tripp, M.L. Hair, J. Phys. Chem. 97 (1993) 5693.
[45] F. Boroumand, H. van den Bergh, Anal. Chem. 66 (1994) 2260.
[46] W. Hertl, M.L. Hair, J. Phys. Chem. 72 (1968) 4676.
[47] K. Klier, J.H. Shen, A.C. Zettlemoyer, J. Phys. Chem. 77 (1973) 1458.
[48] A.C. Zettlemoyer, H.H. Hsing, J. Colloid Interface Sci. 58 (1977) 263.
[49] S.G. Bush, J.W. Jorgenson, M.L. Miller, R.W. Linton, J. Chromatogr. 260 (1983) 1.
[50] M.L. Miller, R.W. Linton, S.G. Bush, J.W. Jorgenson, Anal. Chem. 56 (1984) 2204.
[51] D.B. Marshall, D.E. Connolly, Anal. Lett. 18 (1985) 995.
[52] S.G. Bush, J.W. Jorgenson, J. Chromatogr. 503 (1990) 69.
[53] J.L. Koenig, P.T.K. Shih, P. Lagally, Mater. Sci. Eng. 20 (1975) 127.
[54] B.A. Morrow, J. Phys. Chem. 81 (1977) 2663.
[55] B.A. Morrow, A.H. Hardin, J. Phys. Chem. 83 (1979) 3135.
[56] R.L. White, A. Nair, Appl. Spectrosc. 44 (1990) 69.
[57] J.B. Bates, R.W. Hendricks, L.B. Shaffer, J. Chem. Phys. 61 (1974) 4163.
[58] R.H. Stolen, G.E. Walrafen, J. Chem. Phys. 64 (1976) 2623.
[59] C.M. Hartwig, L.A. Rahn, J. Chem. Phys. 67 (1977) 4260.
[60] G.E. Walrafen, P.N. Krishnan, S.W. Freiman, J. Appl. Phys. 52 (1981) 2832.
[61] G.E. Walrafen, M.S. Hokmabadi, N.C. Holmes, W.J. Nellis, S. Henning, J. Chem. Phys. 82 (1985) 2472.
[62] G.E. Walrafen, M.S. Hokmabadi, N.C. Holmes, J. Chem. Phys. 85 (1986) 771.
[63] T.A. Egerton, A.H. Hardin, Y. Kozirovsk, N. Sheppard, J. Catal. 32 (1974) 343.
[64] M.B. Sayed, R.P. Cooney, J. Colloid Interface Sci. 91 (1983) 552.
[65] K. Witke, Appl. Spectrosc. 36 (1982) 471.
[66] M.B. Sayed, R.P. Cooney, J. Colloid Interface Sci. 96 (1983) 381.
[67] S.F. Simpson, J.M. Harris, J. Phys. Chem. 94 (1990) 4649.
[68] R.E. Majors, M.J. Hopper, J. Chromatogr. Sci. 12 (1974) 767.
[69] G.E. Berendsen, L. de Galan, J. Liq. Chromatogr. 1 (1978) 561.
[70] H.A. Claessens, C.A. Cramers, J.W. De Haan, F.A. Den Otter, Chromatographia 20 (1985) 582.
[71] V.M. Rangnekar, P.B. Oldham, Spec. Lett. 22 (1989) 993.
[72] J.W. de Haan, H.M. van den Bogaert, J.J. Ponjeé, L.J.M. van de Ven, J. Colloid Interface Sci. 110 (1986) 591.
[73] H. Hemetsberger, W. Maasfeld, H. Ricken, Chromatographia 9 (1976) 303.
[74] T.S. Den, A.A. Kettrup, Chromatographia 19 (1984) 231.
[75] A. Chartier, C. Gonnet, D. Morel, J.L. Rocca, J. Serpinet, J. Chromatogr. 438 (1988) 263.
[76] L.W. Yu, T.R. Floyd, R.A. Hartwick, J. Chromatogr. Sci. 24 (1986) 177.
[77] V.A. Basiuk, E.G. Khil'chevskaya, Anal. Chim. Acta 255 (1991) 197.
[78] N. Watanabe, Chem. Lett. (1981) 1373.
[79] J.N. Akanya, D.R. Taylor, Chromatographia 28 (1989) 212.
[80] C. Pidgeon, U.V. Venkataram, Anal. Biochem. 176 (1989) 36.
[81] R.J. Markovich, J.M. Stevens, C. Pidgeon, Anal. Biochem. 182 (1989) 237.
[82] R.J. Markovich, X. Qiu, D.E. Nichols, C. Pidgeon, B. Invergo, F.M. Alvarez, Anal. Chem. 63 (1991) 1851.
[83] V.A. Basiuk, A.A. Chuiko, J. Chromatogr. 521 (1990) 29.
[84] J.E. Sandoval, J.J. Pesek, Anal. Chem. 61 (1989) 2067.
[85] J.E. Sandoval, J.J. Pesek, Anal. Chem. 63 (1991) 2634.
[86] J.J. Pesek, M.T. Matyska, J. Chromatogr. A 687 (1994) 33.
[87] J.J. Pesek, J.E. Sandoval, M. Su, J. Chromatogr. 630 (1993) 95.
[88] J.J. Pesek, V.H. Tang, Chromatographia 39 (1994) 649.
[89] J.J. Pesek, S.A. Swedberg, J. Chromatogr. 361 (1986) 83.
[90] J. Pesek, G. Guiochon, J. Chromatogr. 395 (1987) 1.
[91] J. Pesek, T. Cash, Chromatographia 27 (1989) 559.
[92] J.J. Pesek, M.A. Vidensek, M. Miller, J. Chromatogr. 556 (1991) 373.
[93] J.J. Pesek, E.J. Williamsen, Trends Anal. Chem. 11 (1992) 259.
[94] L.C. Sander, J.B. Callis, L.R. Field, Anal. Chem. 55 (1983) 1068.

[95] B.R. Suffolk, R.K. Gilpin, Anal. Chem. 57 (1985) 596.
[96] P. Guyot-Sionnest, R. Superfine, J.H. Hunt, Y.R. Shen, Chem. Phys. Lett. 144 (1988) 1.
[97] T. Ohtake, N. Mino, K. Ogawa, Langmuir 8 (1992) 2081.
[98] K. Jinno, J. Wu, M. Ichikawa, I. Takata, Chromatographia 37 (1993) 627.
[99] W.R. Thompson, J.E. Pemberton, Anal. Chem. 66 (1994) 3362.
[100] R.G. Snyder, J. Chem. Phys. 47 (1967) 1316.
[101] R.L. Jernigan, P.J. Flory, J. Chem. Phys. 50 (1969) 4165.
[102] P.J. Flory, Statistical Mechanics of Chain Molecules, Interscience, New York, 1969.
[103] D.J. Gardiner, in: D.J. Gardiner, P.R. Graves (Eds.), Practical Raman Spectroscopy, Springer-Verlag, New York, 1989, pp. 1.
[104] K. Kimata, N. Tanaka, T. Araki, J. Chromatogr. 594 (1992) 87.
[105] J. Nawrocki, D.L. Moir, W. Szczepaniak, Chromatographia 28 (1989) 143.
[106] K. Kimata, K. Iwaguchi, S. Onishi, K. Jinno, R. Eksteen, K. Hosoya, M. Araki, N. Tanaka, J. Chromatogr. Sci. 27 (1989) 721.
[107] Y. Ohtsu, Y. Shiojima, T. Okumura, J. Koyama, K. Nakamura, O. Nakata, K. Kimata, N. Tanaka, J. Chromatogr. 481 (1989) 147.
[108] P.C. Sadek, C.J. Koester, L.D. Bowers, J. Chromatogr. Sci. 25 (1987) 489.
[109] M. Verzele, M. De Potter, J. Ghysels, J. High Resolut. Chromatogr. Chromatogr. Commun. 2 (1979) 151.
[110] C.K. Chong, C. Shen, Y. Fong, J. Zhu, F. Yan, S. Brush, C.K. Mann, T.J. Vickers, Vib. Spectrosc. 3 (1992) 35.
[111] D.R. Lombardi, C. Wang, B. Sun, A.W. Fountain III, T.J. Vickers, C.K. Mann, F.R. Reich, J.G. Douglas, B.A. Crawford, F.L. Kohlasch, Appl. Spectrosc. 48 (1994) 875.
[112] K.B. Sentell, K.W. Barnes, J.G. Dorsey, J. Chromatogr. 455 (1988) 95.
[113] J.N. Kinkel, K.K. Unger, J. Chromatogr. 316 (1984) 193.
[114] G.E. Berendsen, K.A. Pikaart, L. de Galan, J. Liq. Chromatogr. 3 (1980) 1437.
[115] R.E. Majors, LC–GC 14 (1996) 190.
[116] K.B. Sentell, A.N. Henderson, Anal. Chim. Acta 246 (1991) 139.
[117] D. Lin-Vien, N.B. Colthup, W.G. Fateley, J.G. Grasselli, The Handbook of Infrared and Raman Characteristic Frequencies of Organic Molecules, Academic Press, New York, 1991.
[118] R.M. Silverstein, G.C. Bassler, T.C. Morrill, Spectrometric Identification of Organic Compounds, 5th ed., John Wiley and Sons, New York, 1991.
[119] D.M. Bliesner, K.B. Sentell, Anal. Chem. 65 (1993) 1819.
[120] Z. Li, S.C. Rutan, S. Dong, Anal. Chem. 68 (1996) 124.
[121] R.K. Iler, J. Chromatogr. 209 (1981) 341.
[122] L.R. Snyder, H. Poppe, J. Chromatogr. 184 (1980) 363.